CrossMark

ORIGINAL ARTICLE

Asbestiform and non-asbestiform morphologies in a talc and vermiculite mine from the province of Córdoba (Argentina): a case study

Leticia Lescano[1,2] · Francisco Locati[3] · Jorge Sfragulla[4] · Silvina Marfil[1,2] · Aldo Bonalumi[4] · Pedro Maiza[1]

Abstract In this work, a talc and vermiculite mine from the province of Córdoba (Argentina) was investigated with special emphasis on the occurrence of asbestiform and non-asbestiform phases. The meta-ultramafic rock was studied by a multimethodological approach, complementing field studies with petrographic-mineralogical, compositional and morphological analyses. Samples were examined by stereomicroscopy, polarizing light microscopy, SEM–EDS, XRD, DSC-TGA and FTIR. Complementary, compositional and textural analyses were performed with FE-SEM–EDS and EPMA. Talc-rich veins with a laminar and fibrous appearance were at first recognized. However, the fibrous morphology observed both in the field and by microscopy is due to an apparent habit because of the sample orientation. To avoid erroneous interpretations, studies by secondary electron images (SEM) are fundamental to carrying out this type of analysis. Tremolite was identified in different zones of the outcrop; however, only ∼40% of the crystals located in the vermiculite zone have dimensions to be considered as asbestiform fibres in the range of respirable particles. In these types of complex deposits affected by superimposed metamorphic, igneous and deformational events, multimethodological approaches are necessary to develop models of occurrence of asbestiform morphologies that may be applicable to other with similar characteristics.

Keywords Meta-ultramafic rock · Tremolite · Asbestos · Talc · Argentina

✉ Leticia Lescano
leticia.lescano@uns.edu.ar

1   Departamento de Geología, Universidad Nacional del Sur (UNS), San Juan 670, 8000 Bahía Blanca, Argentina

2   CGAMA (Comisión de Investigaciones Científicas de la Prov. de Bs. As-UNS), Buenos Aires, Argentina

3   CICTERRA (CONICET - UNC), Av. Vélez Sarsfield 1611, X5016GCA Córdoba, Argentina

4   Secretaría de Minería (Provincia de Córdoba) y Facultad de Cs. Exactas, Físicas y Naturales, Universidad Nacional de Córdoba, Córdoba, Argentina

Introduction

The meta-ultramafic rocks of the province of Córdoba (Argentina) have been exploited for decades, especially for the production of dark green to black aggregates for the manufacture of mosaics and as fluxes in steelworks in partial replacement of calcite and dolomite. They were also exploited to obtain chromite, talc, vermiculite and asbestos, but with the exception of serpentinite, production was scarce, and the products were of medium quality.

An extensive and large belt is recognized in the eastern sector of the western ultramafic belt, with development of talc bodies associated with vermiculite (Rosarito, La Cuarta, Juancho mines and others) and the ultramafic bodies from Pampa del Agua Fría to Candelaria (Bonalumi et al. 2014).

The Rosarito mine was exploited until the end of the 1980s, with the extraction of second-grade talc and in some sectors, vermiculite. Although it is currently abandoned, it is important to carry out detailed studies of the deposit to determine the occurrence of asbestiform minerals that may be present in the talc ore or associated with vermiculite-rich belts, bearing in mind that there are records on the presence of these morphologies in ultramafic rocks of the province of Córdoba (Lescano et al. 2011, 2013, 2014). This will help advance the design of a geological model

🙂 Springer

that can be extrapolated, in order to identify this type of morphology in similar outcrops, considering that the production, import, commercialization and use of asbestos fibres, and products that contain amphiboles (Resolution No. 845/2000) and chrysotile (Resolution No. 823/2001) varieties have been banned in Argentina since 2003 (Rodríguez 2004).

The presence of asbestiform minerals as impurities in talc and vermiculite deposits and their potential impact on human health have been a subject of study and debate for more than 40 years worldwide (e.g. Van Gosen et al. 2004; Antao et al. 2012 and references therein). However, it is important to further improve field studies on meta-ultramafic rocks and associated mineralized zones, since a close relationship is expected between the occurrence of asbestiform minerals and the geological history of host rocks (Ross and Nolan 2003; Van Gosen et al. 2004; Vignaroli et al. 2011, 2014; Bloise et al. 2014).

According to the protocols of the World Health Organization (WHO 1986) the evaluation of asbestos fibre content (in air) is limited to those with a length (l) >5 μm, diameter (d) <3 μm and a length to diameter ratio (l/d) ≥3:1, considering those particles to be the most biologically relevant part of the alveolar fraction. The US Occupational Safety and Health Administration (OSHA 1992) uses a similar criterion ($l \geq 5$ μm, $l/d \geq 3$:1) although no definitions are made regarding the diameter. According to the WHO (1986), there is consensus that the maximum limit for the diameter of respirable asbestos particles is 3 μm (cut-off of the alveolar fraction).

Although this paper does not intend to carry out a comprehensive review about the danger associated with fibre dimensions, it is important to analyse some aspects that will contribute to the discussion of the topic. Currently, there is a large amount of literature addressing the hazard level of fibres in the face of the development of carcinogenic diseases such as lung cancer or mesothelioma, mainly based on their size and mineralogy. Those records are based on laboratory studies on animals as well as on epidemiological studies on humans (e.g. Stanton et al. 1981; Berman and Crump 2003, 2008; Loomis et al. 2010; Lippmann 1988, 1994, 2009; Case et al. 2011; Berman 2011). Although the proposed limits vary among the different studies, most of them agree that the hazard is greater for long and thin fibres (Wylie and Candela 2015). In general, a higher toxicity is attributed to those with a length >5 μm (with higher incidence for fibres ≥10 μm long) and diameters up to ~1.5 μm. According to the literature, fibres with diameters up to 1.5 μm are capable of penetrating to sensitive portions of the lung during oral inhalation (ERG 2003; ACSH 2007; Berman and Crump 2003, 2008; Berman 2011). These limits may vary depending on the pathology studied and whether the data

come from laboratory animal studies or epidemiological studies on humans (ERG 2003; Lippmann 2009). Regarding the effect of short fibres (<5 μm), there are studies that recommend taking them into account because they may play a role in the induction of pathologies such as cancer (Dodson et al. 2003; Boulanger et al. 2014; Markowitz 2015), although their bioreactivity and toxicity would be substantially lower compared to long fibres (Berman and Crump 2008; Mossman et al. 2011). From a mineralogical point of view, asbestiform amphiboles are generally more biopersistent than chrysotile and, therefore, more dangerous (Ross et al. 1993). They may lead to the development of mesothelioma (Berman and Crump 2008) because they accumulate and remain unaltered in the lung, while chrysotile tends to dissolve much more rapidly (Gibbons 1998; Sanchez et al. 2009; Gunter et al. 2007).

In Argentina, the criterion proposed by the WHO (1986) for the dimensions of the fibres that should be considered as harmful is within Resolution No. 577/1991 of the Ministry of Labour and Social Security, so it is the one used in this country. Therefore, although the criterion applied could overestimate the number of hazardous asbestiform particles, it is still a conservative decision that includes those fibres of greater toxicity. In addition, although at international level, there are some proposals to determine the presence of asbestiform minerals in deposits or rock samples (commonly called "Naturally Occurring Asbestos"—NOA, Lee et al. 2008; Harper 2008; Bloise et al. 2016b), based on multimethodological studies (Brown et al. 1979; Berman 2003; Giacomini et al. 2010; Rigopoulos et al. 2010; Vignaroli et al. 2014; Marescotti et al. 2014), the Argentine regulation does not include concrete specifications in this sense.

In this work, a multimethodological approach is taken, complementing field studies with petrographic-mineralogical, compositional and morphological analyses of a talc and vermiculite mine from the province of Córdoba (Argentina). Different alteration zones in the meta-ultramafic rock were recognized and studied with special emphasis on the presence of asbestiform and non-asbestiform phases, in order to develop a model applicable to other exploitation areas in the region.

Location and geological setting

The study area includes the Rosarito mine, located in the Cuesta de Matacaballos, 6 km northwest of the town of Molinari, in the province of Córdoba (Argentina) (latitude: 31°10′20″S, longitude: 64°31′14″W).

The sector is emplaced in the El Perchel-Pampa de Olaen block, limited to the east by the Punilla valley and to the west by the inverse fault (east dip) El Perchel (Fig. 1).
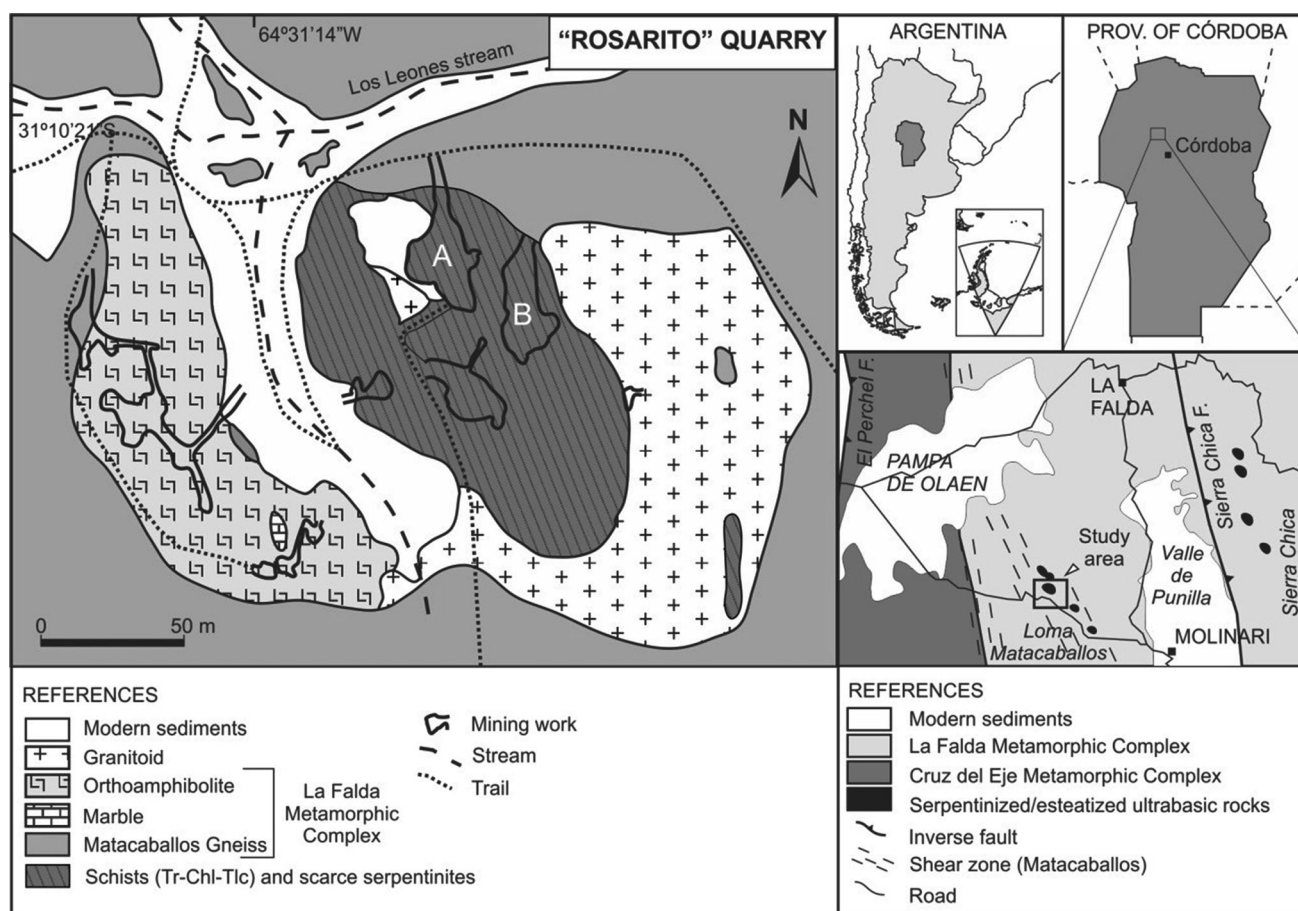
Fig. 1 Location of the study area in the province of Córdoba (Argentina) and geological scheme of the Rosarito mine. A and B: sampled works. Modified from Sfragulla and Moreno (1985)

In the central part of this block, a series of N-NW to N-S shear belts define the Matacaballos shear zone, which separates the La Falda Metamorphic Complex to the east from the Cruz del Eje Metamorphic Complex to the west.

Bonalumi et al. (1999) recognized a diaphthorite with muscovite-chlorite-ilmenite in this area, which they called Matacaballos Gneiss. It is a rock with gneissic or coarse grain schist appearance, dark grey to green with leucocratic bands, with a greenschist paragenesis formed by an intense retrogradation of higher grade association that remains as relict (biotite–garnet–sillimanite–plagioclase–potassium feldspar).

In the "Cuesta de Matacaballos" and associated with the diaphthorite, a series of steatized ultramafic bodies (Olaen ultramafic rocks) of lenticular form with variable strike (N 300°–340°) and general dip $\sim 60°$ SW (Cuervo 1988) is recognized. The Rosarito mine was developed on one of these bodies and corresponds to a series of open-pit mining works with variable dimensions ranging from 20 to 100 m in length, some of them in an advanced grade of deterioration, making it difficult to determine the field relationships.

The mineralized body has ovoid shape with $\sim$ N 330° strike and comprises a group of metamorphosed ultramafic rocks (mainly tremolite–chlorite and talc–chlorite schists with subordinate serpentinites) associated with marbles and amphibolites to the west.

In the northern area, the body is in contact with the diaphthorite and to the east a pink granitoid intrudes the metamorphic complex. In the meta-ultramafic rock, serpentine group minerals, prismatic and acicular amphiboles, massive talc and talc in veins with fibrous appearance, chlorite, and pyrite together with other opaque minerals can be identified.

Materials

The Rosarito mine has several inactive exploitation fronts, generally covered by abundant vegetation, buried and with eddy sectors, so the sampling was focused on workings A and B (Fig. 1). Twenty-eight samples were taken from the different altered zones as well as from the lithologies in contact zones.

Workings A consist of a trench with N-S strike on the meta-ultramafic rock (serpentinized and steatized). In the central sector, a zone rich in fine-grained talc, the ore exploited in the past, is observed. This zone is not regular and appears as whitish spots when the talc content is higher or is concentrated in sheared bands. In different areas of the mine (including this ore area), talc veins of fibrous appearance are also in contact with sectors rich in massive talc and chlorite.

Towards the west, the body is in contact with a fine-grained granitoid apophysis that outcrops further east (Fig. 1). In this sector, the content of light green amphiboles in the steatized body is higher (amphibole zone), and in contact with the igneous body a vermiculite zone has developed, represented by discontinuous bands filled with this mineral.

Vermiculite filling fractures is also recognized in other sectors of the body, with an increase in the amphibole content on both sides of the fractures, followed by a talc-enriched zone, similar to that developed in contact with the granitic body. Within the vermiculite zone, discontinuous lenses of Qz + Kfs + Tr and Dol + Chl are observed. In addition, discordant veins of quartz and carbonates were identified in different parts of the steatized body. Workings B are located in the upper sector of the hill (N-S strike) and

are geologically similar to workings A. Figure 2 shows a simplified scheme of the distribution of the alteration zones.

Methods

Samples were studied by stereomicroscopy with an Olympus trinocular SZ-PT stereomicroscope on natural surfaces and by polarizing light microscopy on thin sections with an Olympus trinocular B2-UMA microscope. X-ray diffraction (XRD) studies were performed with a Rigaku D-Max III-C diffractometer with Cu K$\alpha_{1,2}$ ($\lambda = 1.541840$ Å) radiation filtered with a graphite monochromator in the diffracted beam. Diffraction patterns were recorded at 35 kV and 15 mA, between 3 and 60° 2θ (steps of 0.04° 2θ and 1 s counting time per step).

Complementary, compositional and textural analyses were performed on carbon-coated polished thin sections (abrasive up to 1 μm), with a high-resolution field emission scanning electron microscope (FE-SEM) Carl Zeiss Field Emission-Σigma coupled with an energy-dispersive X-ray spectrometer (EDS). Compositional maps were obtained working at 15 kV and 0.1–0.2 nA. Quantitative chemical analyses were performed with an electron probe micro-
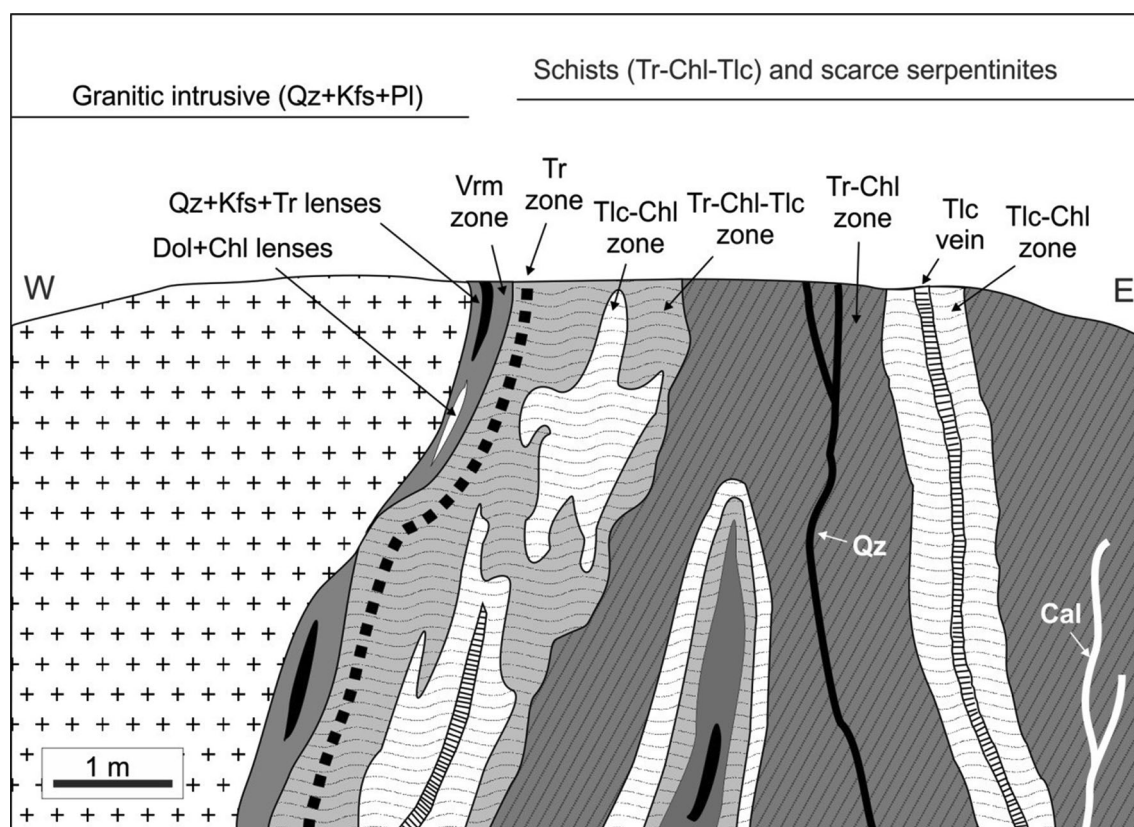

Fig. 2 Simplified scheme of the alteration zones in the meta-ultramafic rock

analyser (EPMA) JEOL JXA 8230 equipped with three wavelength-dispersive spectrometers (WDS) and one EDS. Conditions were set at 15 kV and 20 nA. Analyses were carried out using a beam diameter of 5 μm, counting 10 s in the peak and 5 s in the background on both sides (5 and 2.5 s for potassium, respectively). The standards used were albite (Na), MgO (Mg), anorthoclase (Al, Si for talc), wollastonite (Ca), olivine-forsterite (Si for chlorite and tremolite), ilmenite (Ti), sodalite (Cl), apatite (P), orthoclase (K), chromite (Cr), rhodonite (Mn), olivine-fayalite (Fe) and nickeline (Ni). Correction for matrix effects was made using the $\phi(\rho z)$ ("phi-rho-z") algorithm.

In addition, studies by simultaneous differential scanning calorimetry and thermogravimetric analysis (DSC-TGA), and Fourier transform infrared spectroscopy (FTIR) were performed in zones rich in talc (talc of fibrous appearance in veins and massive talc in Tlc–Chl zone) to determine the presence of accessory phases. DSC-TGA diagrams were obtained with TA Q600 analyser under inert atmosphere at a heating rate of 10 °C/min from ambient temperature up to 1100 °C. FTIR spectra were recorded with Nicolet 520 spectrometer. One mg of the samples was dispersed in 100 mg KBr and pressed in pellets. For each spectrum, 100 scans were recorded in the 400–4000 cm^{-1} spectral range with a resolution of 4 cm^{-1} in absorbance mode.

Finally, morphological analyses of acicular and fibrous phases were conducted. First, the material was separated under the stereomicroscope and then it was analysed by petrography and SEM with an EVO 40XVP microscope on gold-coated natural surfaces. Secondary electron images were obtained working at 10 kV. With optical microscopy particles up to ∼1 μm can be analysed, while by SEM particles up to ∼0.1 μm can be visualized. Therefore, when complemented, these two techniques are useful to characterize the morphologies of the particles (Gunter et al. 2007).

In this work, abbreviations after Whitney and Evans (2010) were used.

Results

Textural and mineralogical characterization

Main body (tremolite–chlorite and tremolite–chlorite–talc zone)

The body is mainly composed of a set of tremolitic–chlorite schists (tremolite–chlorite zone) (Fig. 3a), where the main paragenesis is tremolite + chlorite with talc in variable proportions. As accessory phases, opaque minerals and scarce antigorite are recognized. Chlorite is arranged in

sheets (∼500 μm) more or less flexed and roughly oriented.

Near the ore zone, the talc content increases (tremolite–chlorite–talc zone) and appears as sheets or packets intergrown with chlorite of similar grain size (Fig. 3b).

The tremolite appears superimposed on the chlorite or chlorite + talc association as euhedral and elongated acicular prisms of larger grain size (250 μm to 1.5 mm long and 10–250 μm in diameter), without a defined orientation or with slight orientation in some sectors.

In general, they are highly fractured in the direction of the cleavage planes or perpendicular to the elongation of the crystals. By means of backscattered electron images and compositional maps (Si, Al, Ca), the intergrowth between chlorite and talc, and the calcium amphiboles that crosscut the foliation of the rock (Fig. 3c–f) is clearly observed.

In restrained sectors, rounded edge serpentinites composed mainly of antigorite of planar habit and opaque minerals (with tremolite, chlorite and talc as subordinate phases) are recognized. Finally, discordant veins of quartz, calcite and talc of fibrous appearance are observed.

In the central sector of the workings and heterogeneously distributed, a talc–chlorite schist (talc–chlorite zone) with marked schistosity and strong evidence of folding is identified. This area represents the mine ore, and the paragenesis talc + chlorite (±opaque minerals) is recognized. In addition, scarce antigorite almost totally replaced by chlorite is observed. Two different talc morphologies are detected, one formed by sheets (∼500–100 μm) with irregular edges arranged in coarse bands in the direction of the main rock foliation, and the other of very fine grain size (<50 μm) between these bands.

Chlorite (∼200 μm) is mainly associated with coarser talc, as flexed or fan-shaped sheets, although some fine-grained talc is also observed between the chlorite sheets. Opaque minerals are abundant and usually of cubic habit (≤100 μm).

Talc-rich veins of fibrous appearance were recognized in the talc–chlorite zone (talc ore) and crosscutting other sectors of the meta-ultramafic body, the latter with evidence of alteration halos (Tlc + Chl) on both sides of the veins (Fig. 4a–c). The massive and fine-grained talc in contact with the veins usually appears partially stained due to the presence of iron oxides and is associated with chlorite and relics of antigorite. Talc inside veins is associated with scarce chlorite (Fig. 4d, e) and has laminar to fibrous appearance with crystals ∼100 μm–1 mm long growing almost perpendicular to the walls of the vein (Fig. 4a–c). Talc of fibrous appearance is also observed inside the veins forming fan-shaped arrangements (Fig. 4f).

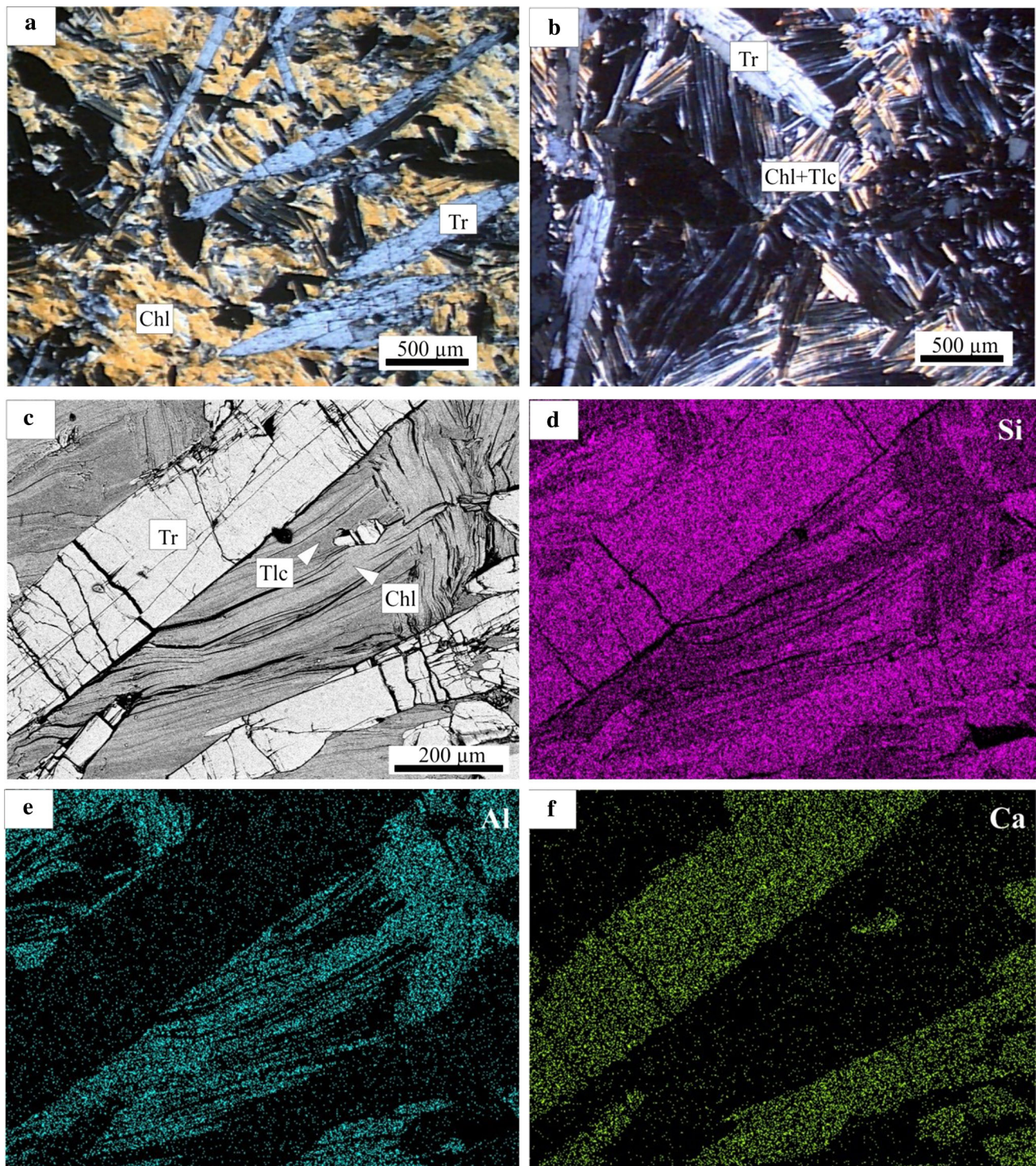Figure 5 shows the XRD patterns of the three zones analysed. The increase in the proportion of talc with

Fig. 3 Tremolitic–chlorite schist. **a** and **b** Photomicrographs (cross-polarized light—XPL) of the schist in Tr–Chl zone (**a**) and Tr–Chl–Tlc zone (**b**). **c–f** FE-SEM–EDS. Backscattered electron image (**c**) of the schist in Tr–Chl–Tlc zone and compositional maps of Si (**d**), Al (**e**) and Ca (**f**) in the same sector

respect to chlorite and tremolite can be observed from the Tr–Chl zone to the Tr–Chl–Tlc zone and finally to the Tlc–Chl zone corresponding to the talc ore. It is important to note that in spite of using the same scanning conditions, the diffraction pattern intensity for the latter zone increases significantly because of the higher proportion of talc with respect to the other phases.
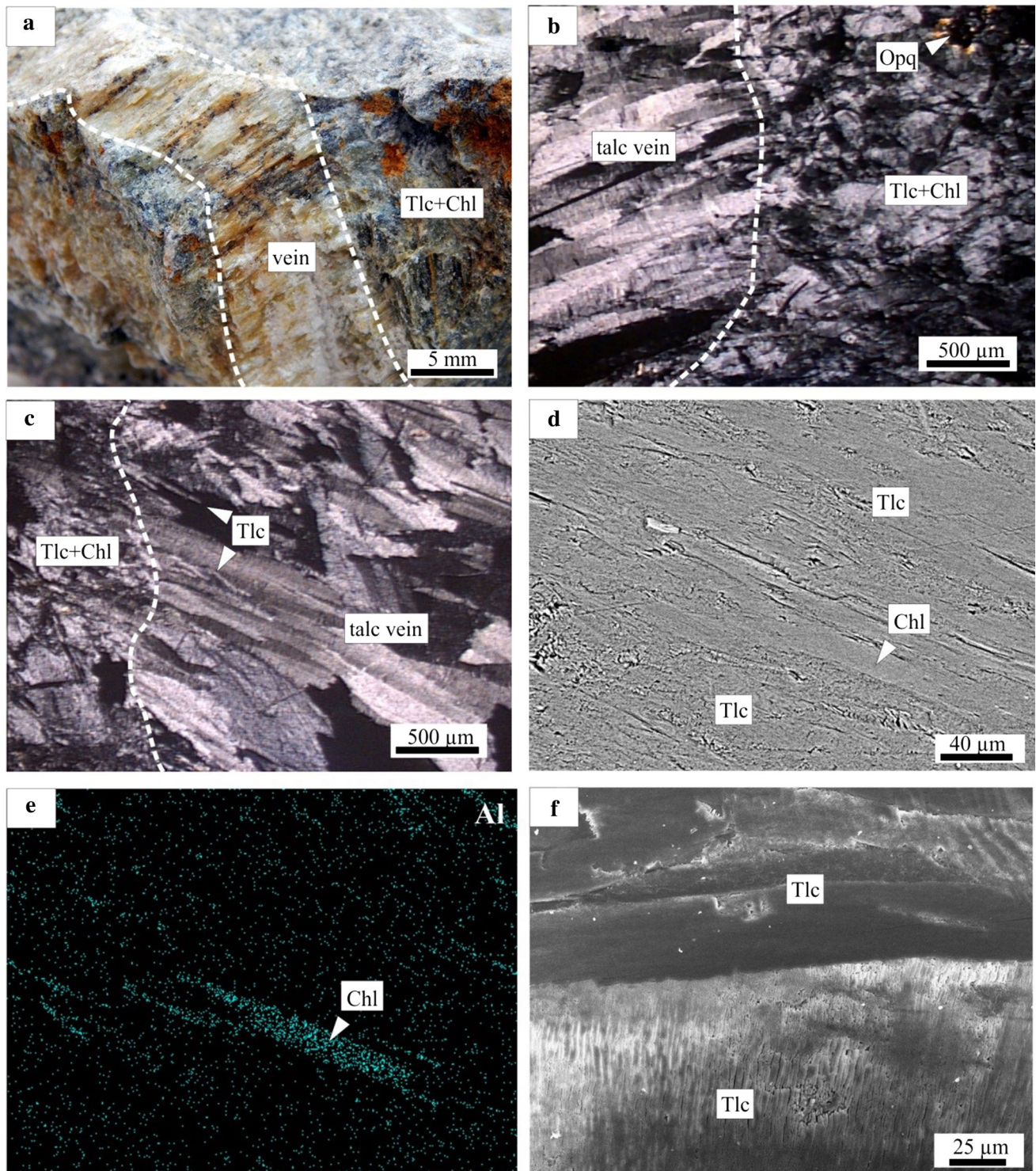
Fig. 4 a Fibrous appearance of talc in vein (stereomicroscopy). b and c Photomicrographs (XPL) of talc vein in contact with massive talc + chlorite. Talc in vein appears as elongated laminar crystals and has fibrous appearance (white arrows). d–f FE-SEM–EDS. d Backscattered electron image of the interior of the talc vein. e Compositional map of Al in the same sector. f Secondary electron image (on thin section) of a talc-rich sector with laminar (above) and fibrous (below) appearance
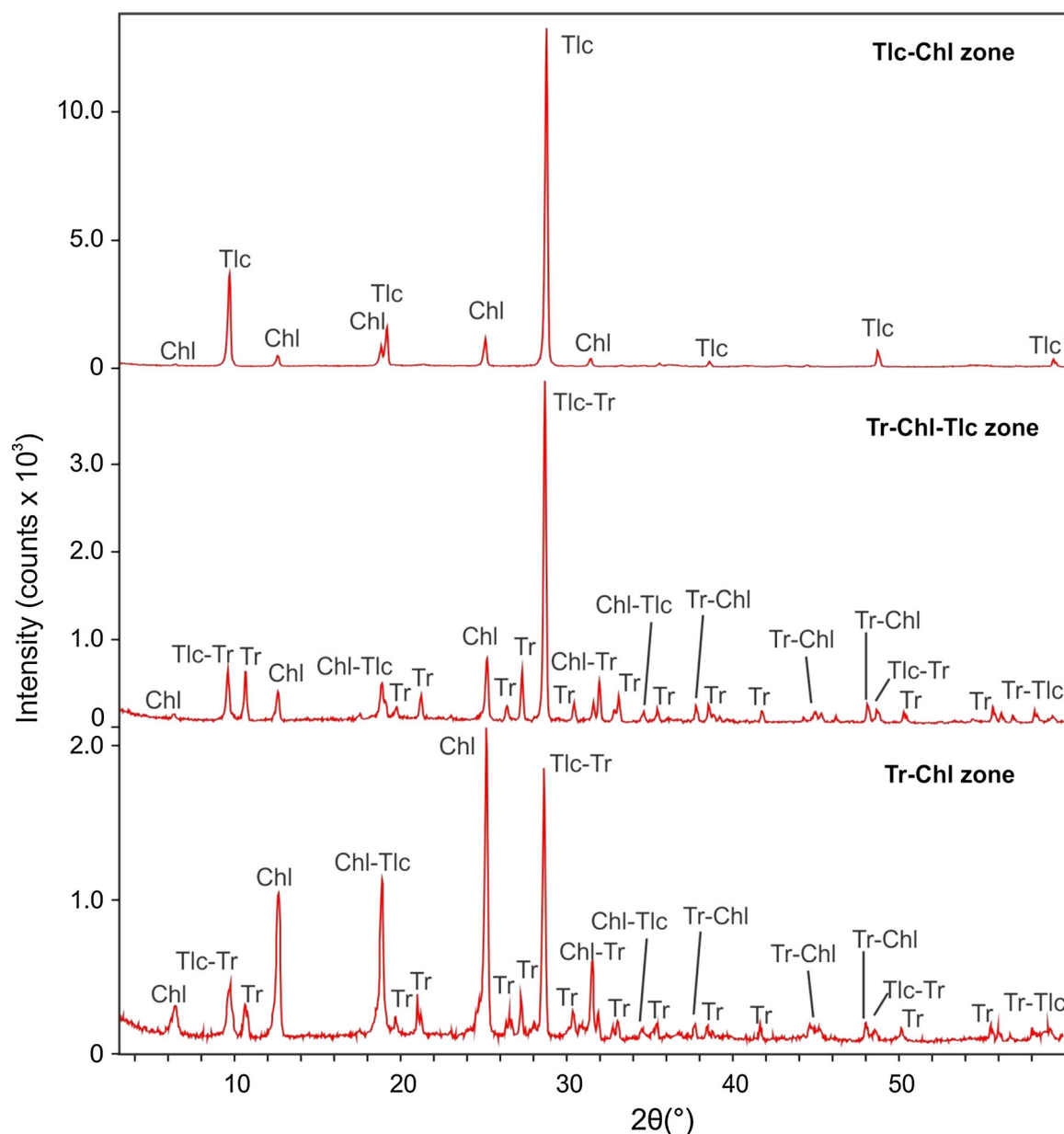
Fig. 5 XRD patterns of Tlc–Chl, Tr–Chl–Tlc and Tr–Chl zones

Granite intrusive and associated zones

Towards the west of workings A an apophysis of the granitoid that outcrops further east can be observed. It is a pink granite of medium to fine grain size (1.5–0.5 mm), of holocrystalline hypidiomorphic texture, composed of potassium feldspar and plagioclase (subordinate) and minor amount of quartz. Zircon and magnetite are the main accessory minerals (Fig. 6a). The feldspars are highly altered to illite/kaolinite mainly associated with goethite. Additionally, some sectors rich in chlorite are also detected. Fissures filled with iron oxides are observed, and associated with these sectors muscovite crystals that can

reach ∼200 μm can be identified. In some areas, the granite has pegmatite texture.

In the contact between the granitic intrusive and the schists (Tr–Chl ± Tlc), a black to brown micaceous belt is observed. It is composed mainly of well-crystallized vermiculite (vermiculite zone), with well-developed crystals (ranging from millimetres to centimetres), suboriented and flexed forming packets of stacked sheets. Towards the edges, the crystals are greenish and are associated with calcite, chlorite, talc and tremolite crystals, the latter of fibrous morphology with very fine crystals <250 μm long (Fig. 6b, c).
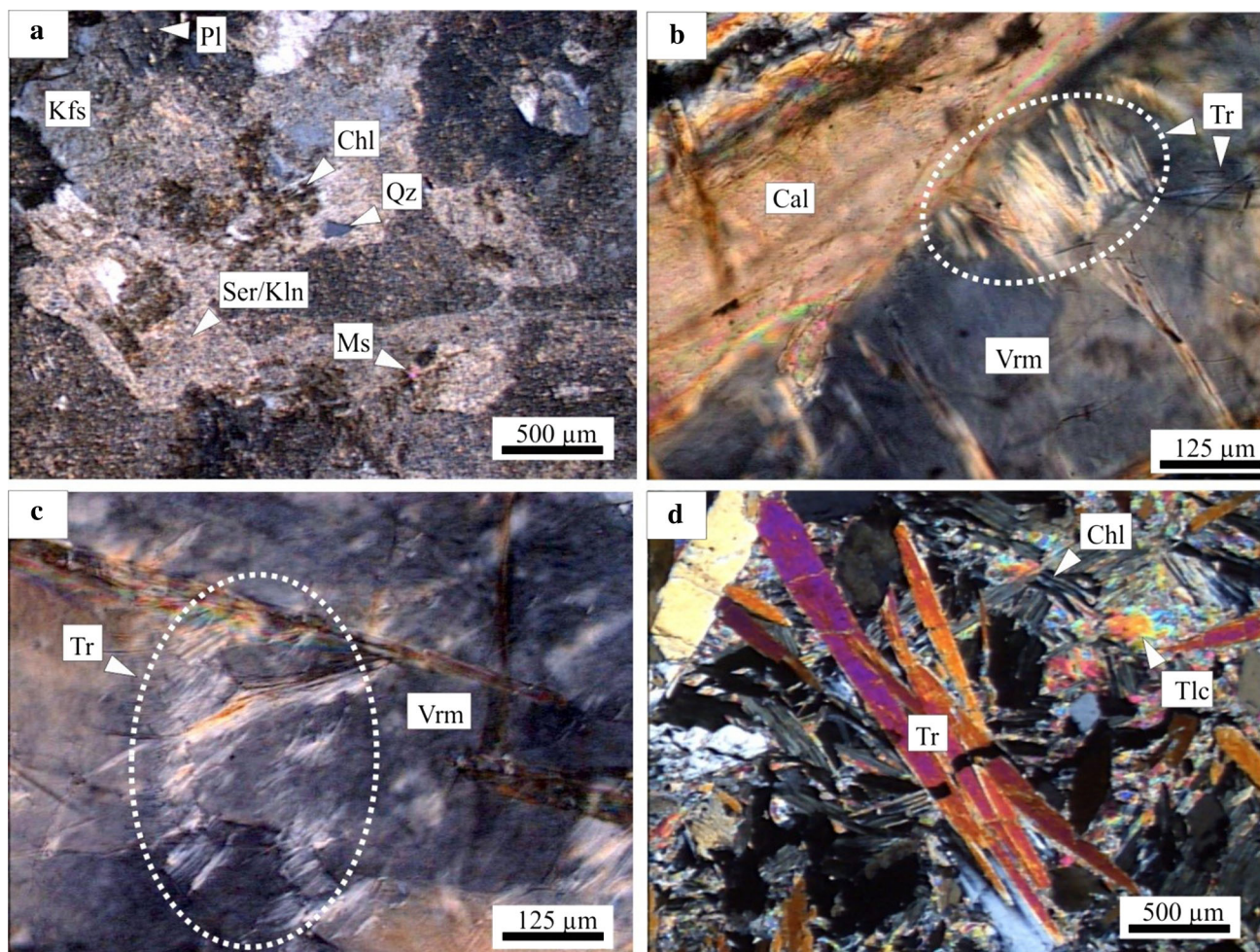
Fig. 6 Photomicrographs (XPL). **a** Altered granitoid. **b** and **c** Fibrous tremolite between vermiculite sheets (vermiculite zone). **d** Tremolitic schist (tremolite zone) in contact with the vermiculite zone

In discrete sectors, the original biotite is still recognized. Between vermiculite packets, quartz and potassium feldspar lenses associated with tremolite fibres are observed. Lenses composed of dolomite and chlorite are also recognized. In the external sectors of the vermiculite packets and in some small pockets, iron oxides are abundant.

In contact with the vermiculite zone, the tremolitic–chlorite schists (±talc) show a strong growth of tremolite (tremolite zone) of very good crystalline development (Fig. 6d), prismatic to acicular habit, and sizes ranging from 450 μm up to 3.5 mm long (in some sectors crystals up to 1 cm were observed, although very locally) and 40–500 μm in diameter. The tremolite has no definite orientation and is associated with packets of chlorite and fine-grained intergranular talc.

Mineral chemistry of the main phases recognized

Table 1 lists the composition of talc identified in Tr–Chl–Tlc and Tlc–Chl zones, and inside the veins. A decrease in iron content in this mineral from the Tr–Chl–Tlc zone to the talc vein is observed ($\sim$2.83 to $\sim$1.64 wt% FeO), accompanied by a small increase in the content of magnesium ($\sim$29.24 to $\sim$29.90 wt% MgO). Similarly to iron, nickel also decreases, although the variation is lower ($\sim$0.24 to $\sim$0.12 wt% NiO).

Bloise et al. (2016a) reported that the pathogenic effects of asbestos are related to the dimension, biopersistence and chemical composition of the fibres (mainly Cr, Ni and Mn).

Table 2 shows the composition at the centre and edge of prismatic and acicular tremolite crystals in the Tr–Chl–Tlc zone. There are no significant compositional variations in the same crystal in the two sectors (centre and edge) or between different crystals. The Cr_2O_3 and NiO contents vary, reaching 0.13 and 0.11 wt%, respectively.

Table 3 shows the composition of chlorites in the Tr–Chl–Tlc and Tlc–Chl zones. Although they are all classified as clinochlore, they show some compositional differences. The clinochlore in the Tr–Chl–Tlc zone is poorer in Si and Mg than that in the Tlc–Chl zone (29.15 vs. $\sim$32.12

Table 1 Chemical analyses of talc determined by EPMA

Group	Talc-Pyrophyllite						
Zones	Tr–Chl–Tlc			Tlc–Chl	Tlc in vein		
Mineral	Talc (1)	Talc (2)	Talc (3)	Talc (4)	Talc (5)	Talc (6)	Talc (7)
SiO_2	62.02	62.57	61.70	61.44	62.15	63.77	62.23
TiO_2	b.d.l.	b.d.l.	b.d.l.	b.d.l.	b.d.l.	b.d.l.	b.d.l.
Al_2O_3	0.22	0.15	0.10	0.35	b.d.l.	0.09	b.d.l.
Cr_2O_3	b.d.l.	b.d.l.	b.d.l.	b.d.l.	b.d.l.	b.d.l.	b.d.l.
FeO^a	2.71	2.80	2.97	1.95	1.69	1.63	1.61
MnO	b.d.l.	b.d.l.	0.08	b.d.l.	b.d.l.	b.d.l.	b.d.l.
MgO	29.09	29.54	29.10	30.93	30.03	29.48	30.20
NiO	0.23	0.30	0.20	0.15	0.09	0.12	0.14
CaO	0.03	b.d.l.	b.d.l.	b.d.l.	0.03	0.04	b.d.l.
Na_2O	0.05	0.05	b.d.l.	b.d.l.	b.d.l.	b.d.l.	b.d.l.
K_2O	0.03	b.d.l.	b.d.l.	b.d.l.	b.d.l.	b.d.l.	b.d.l.
P_2O_5	b.d.l.	b.d.l.	b.d.l.	b.d.l.	b.d.l.	b.d.l.	b.d.l.
Cl	b.d.l.	b.d.l.	b.d.l.	b.d.l.	b.d.l.	b.d.l.	b.d.l.
H_2O+^b	4.64	4.69	4.62	4.67	4.65	4.72	4.66
Total	99.02	100.1	98.77	99.49	98.64	99.85	98.84
Structural formula calculated on the basis of 11 oxygen atoms ($O_{10}(OH)_2 = 11$)							
Si	4.005	3.999	4.000	3.944	4.008	4.051	4.005
Al	0.000	0.001	0.000	0.026	0.000	0.000	0.000
ΣT	4.050	4.000	4.000	3.970	4.008	4.051	4.005
Al	0.017	0.011	0.007	0.000	0.000	0.006	0.000
Ni	0.012	0.016	0.011	0.008	0.005	0.006	0.007
Mn^{2+}	0.000	0.000	0.004	0.000	0.000	0.000	0.000
Fe^a	0.146	0.150	0.161	0.105	0.091	0.087	0.087
Mg	2.800	2.815	2.813	2.960	2.887	2.792	2.897
ΣO	2.975	2.992	2.996	3.073	2.983	2.891	2.991
Ca	0.002	0.000	0.000	0.000	0.002	0.002	0.000
Na	0.007	0.007	0.000	0.000	0.000	0.000	0.000
K	0.002	0.000	0.000	0.000	0.000	0.000	0.000
Σ(Ca, Na, K)	0.011	0.007	0.000	0.000	0.002	0.002	0.000
OH	2.000	2.000	2.000	2.000	2.000	2.000	2.000
ΣCations	6.991	6.998	6.996	7.043	6.992	6.945	6.995
Fe(t)/Fe(t) + Mg	0.05	0.05	0.05	0.03	0.03	0.03	0.03
1-(Fe(t)/Fe(t) + Mg)	0.95	0.95	0.95	0.97	0.97	0.97	0.97

(1)–(3) Tr–Chl–Tlc zone; (4) Tlc–Chl zone; (5)–(7) talc in veins. Contents of components expressed as weight per cent of oxides and atoms per formula unit (a.p.f.u.) of talc on the basis of 11 equivalent oxygen atoms

[a] FeO: iron concentration expressed as total FeO; Fe: iron content expressed as Fe^{2+}

[b] H_2O^+ calculated for 2 OH. "b.d.l.": values below the detection limit

wt% SiO_2 and 26.68 vs. ∼33.47 wt% MgO, respectively). However, the clinochlore in the Tr–Chl–Tlc zone has higher Al, Fe, Cr and Ni contents than that in the Tlc–Chl zone (19.67 vs. ∼15.86 wt% Al_2O_3, 11.2 vs. ∼5.1 wt% FeO_{total}, 0.2 vs. ∼0.12 wt% Cr_2O_3 and 0.17 vs. ∼0.09 wt% NiO, respectively).

DSC-TGA and FTIR studies

Figures 7 and 8 show DSC-TGA and FTIR diagrams of talc with fibrous appearance from a vein and massive talc from the Tlc–Chl zone (exploited ore). For the former, DSC-TGA studies (Fig. 7a) show a slow mass loss (0.94%) at 848.55 °C, which is interpreted as the release of

Table 2 Chemical analyses of tremolite in the Tr–Chl–Tlc zone determined by EPMA

Group	Calcic amphiboles					
Analysed sector	Centre				Edge	
Mineral	Tremolite (1)	Tremolite (2)	Tremolite (3)	Tremolite (4)	Tremolite (5)	Tremolite (6)
SiO_2	57.77	58.51	57.05	57.49	57.46	57.31
TiO_2	b.d.l.	b.d.l.	b.d.l.	b.d.l.	b.d.l.	b.d.l.
Al_2O_3	0.76	0.46	0.51	0.47	0.54	0.52
Cr_2O_3	0.13	0.09	b.d.l.	b.d.l.	b.d.l.	0.11
FeO^a	4.02	3.76	3.98	3.96	4.01	3.92
MnO	0.17	0.21	0.20	0.16	0.19	0.16
MgO	22.91	22.61	21.87	22.11	21.99	21.86
NiO	0.09	b.d.l.	b.d.l.	0.08	0.11	b.d.l.
CaO	12.66	12.84	12.81	12.76	12.66	12.76
Na_2O	0.15	0.07	0.12	0.09	0.09	0.08
K_2O	b.d.l.	b.d.l.	b.d.l.	0.03	b.d.l.	0.03
P_2O_5	b.d.l.	b.d.l.	b.d.l.	b.d.l.	b.d.l.	b.d.l.
Cl	b.d.l.	b.d.l.	b.d.l.	b.d.l.	b.d.l.	b.d.l.
H_2O+^b	2.18	2.18	2.18	2.18	2.18	2.18
Total	100.84	100.73	98.72	99.33	99.23	98.93
Structural formula calculated on the basis of 22 oxygen atoms + 2 (OH.F.Cl)						
Si	7.886	7.973	7.955	7.963	7.966	7.967
Al	0.114	0.027	0.045	0.037	0.034	0.033
ΣT	8.000	8.000	8.000	8.000	8.000	8.000
Al	0.009	0.047	0.039	0.039	0.054	0.053
Cr	0.014	0.010	0.000	0.000	0.000	0.012
Ni	0.009	0.000	0.000	0.009	0.012	0.000
Mn^{2+}	0.000	0.000	0.000	0.000	0.000	0.000
Fe^{2+}	0.305	0.351	0.415	0.386	0.390	0.405
Mg	4.662	4.593	4.546	4.565	4.545	4.530
ΣC	4.999	5.001	5.000	4.999	5.001	5.000
Mn^{2+}	0.019	0.024	0.024	0.019	0.022	0.019
Fe^{2+}	0.154	0.078	0.049	0.072	0.075	0.051
Mg	0.000	0.000	0.000	0.000	0.000	0.000
Ca	1.827	1.875	1.914	1.894	1.880	1.901
Na	0.000	0.018	0.013	0.015	0.022	0.022
ΣB	2.000	1.995	2.000	2.000	1.999	1.993
Ca	0.025	0.000	0.000	0.000	0.000	0.000
Na	0.040	0.000	0.018	0.008	0.002	0.000
K	0.000	0.000	0.000	0.005	0.000	0.005
ΣA	0.065	0.000	0.018	0.013	0.002	0.005
A	0.935	1.000	0.982	0.987	0.998	0.995
OH	2.000	2.000	2.000	2.000	2.000	2.000
Σ(T,C,B,A)	15.064	14.996	15.018	15.012	15.002	14.998

(1)–(4) Centre sector; (5)–(6) edge sector. Contents of components expressed as weight per cent of oxides and atoms per formula unit (a.p.f.u.) of calcic amphiboles normalized according to Locock (2014)

[a] FeO: iron concentration expressed as total FeO

[b] H_2O^+ ratio calculated for 2 OH. "b.d.l.": values below the detection limit

Table 3 Chemical analyses of chlorite determined by EPMA

Group	Chlorite		
Zone	Tr–Chl–Tlc	Tlc–Chl	Tlc–Chl
Mineral	Clinochlore (1)	Clinochlore (2)	Clinochlore (3)
SiO_2	29.15	32.49	31.75
TiO_2	b.d.l.	b.d.l.	b.d.l.
Al_2O_3	19.67	15.71	16.02
Cr_2O_3	0.20	0.15	0.09
$Fe_2O_3^a$	0.11	1.27	1.75
FeO^a	11.09	3.31	3.87
MnO	0.30	b.d.l.	b.d.l.
MgO	26.68	33.97	32.98
NiO	0.17	0.08	0.10
CaO	0.08	b.d.l.	b.d.l.
Na_2O	b.d.l.	b.d.l.	b.d.l.
K_2O	b.d.l.	b.d.l.	b.d.l.
P_2O_5	b.d.l.	b.d.l.	b.d.l.
Cl	b.d.l.	b.d.l.	b.d.l.
H_2O^a	12.23	12.66	12.53
Total	99.68	99.64	99.09
Structural formula calculated on the basis of 14 oxygen atoms ($O_{10}(OH)_8 = 14$)			
Si	2.855	3.077	3.036
Al	1.145	0.923	0.964
ΣT	4.000	4.000	4.000
Al	1.125	0.830	0.842
Cr	0.015	0.011	0.007
Ni	0.013	0.006	0.008
Mn^{2+}	0.025	0.000	0.000
Fe^{3+}	0.008	0.091	0.126
Fe^{2+}	0.909	0.263	0.309
Mg	3.895	4.795	4.702
ΣO	5.990	5.996	5.994
in O site	0.010	0.004	0.006
Ca (Oct.) interlayer	0.008	0.000	0.000
OH	8.000	8.000	8.000
ΣCations	9.998	9.996	9.994
Fe(t)/Fe(t) + Mg	0.191	0.069	0.085

(1) Tr–Chl–Tlc zone; (2)–(3) Tlc–Chl zone. Contents of components expressed as weight per cent of oxides and atoms per formula unit (a.p.f.u.) of standardized chlorites according to Yavuz et al. (2015)

[a] FeO values measured were 11.19, 4.46 and 5.44 (wt%), which were then recalculated together with H_2O and Fe_2O_3 by stoichiometry. "b.d.l.": values below the detection limit

adsorbed water, and then a faster mass loss of 4.4% at 1032.85 °C, which is attributed to dehydroxylation and decomposition of the talc structure (Wesolowski 1984; Földvári 2011). The massive talc has a pattern similar to the fibrous one, although an additional mass loss (1.18%) is observed between 536 and 644 °C, which would be attributed to the dehydroxylation of the "brucite sheet" of chlorite, as proposed by Villieras et al. (1994) (Fig. 7b).

These authors also mentioned a mass loss between ∼600 and ∼800 °C, probably due to the dehydroxylation of the 2:1 layers of chlorite, which would overlap with talc in that region.

Figure 10 shows the FTIR spectra of both phases superimposed, and Table 4 lists the assignment of absorption bands for both samples according to Petit et al. (2004), Parry et al. (2007) and Tan et al. (2012).
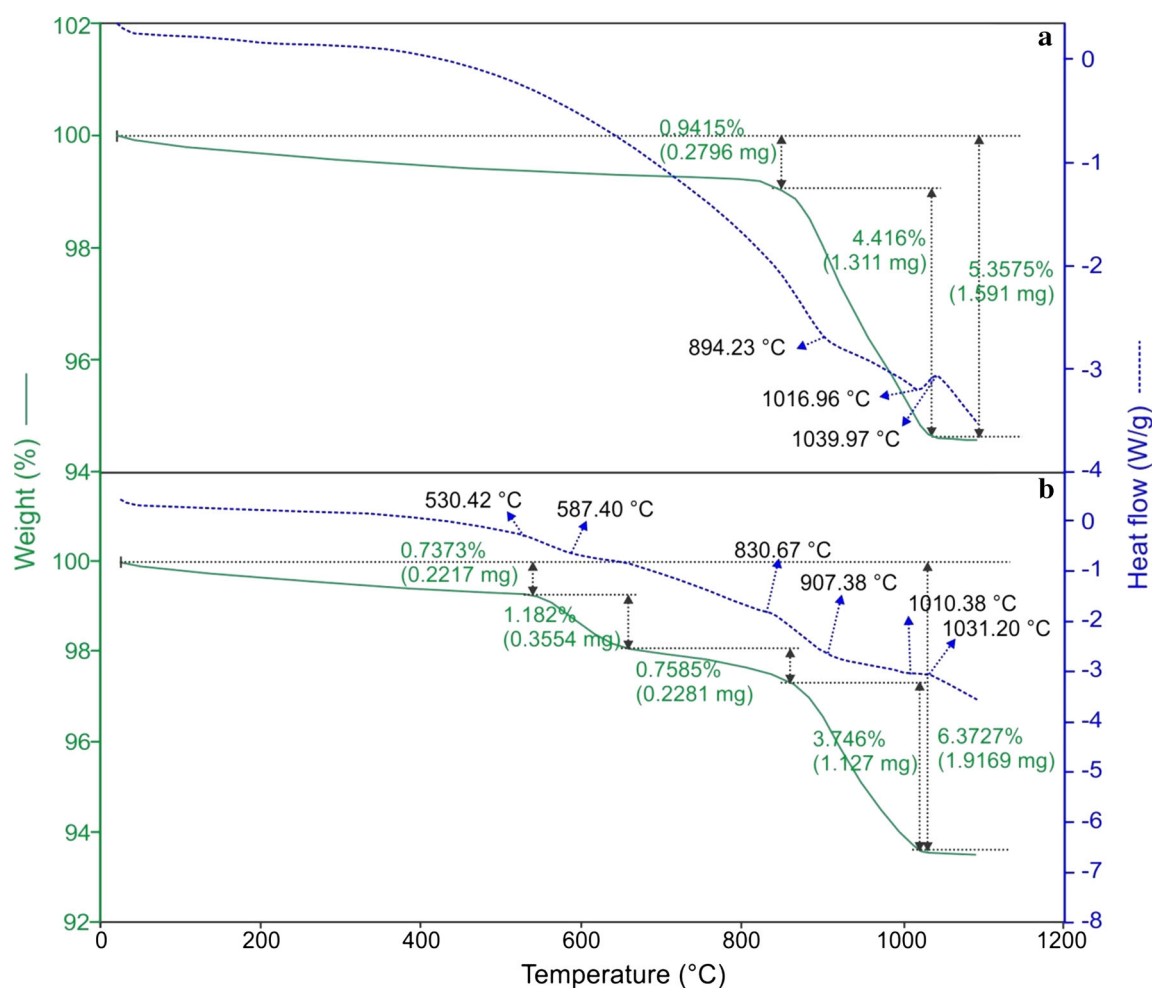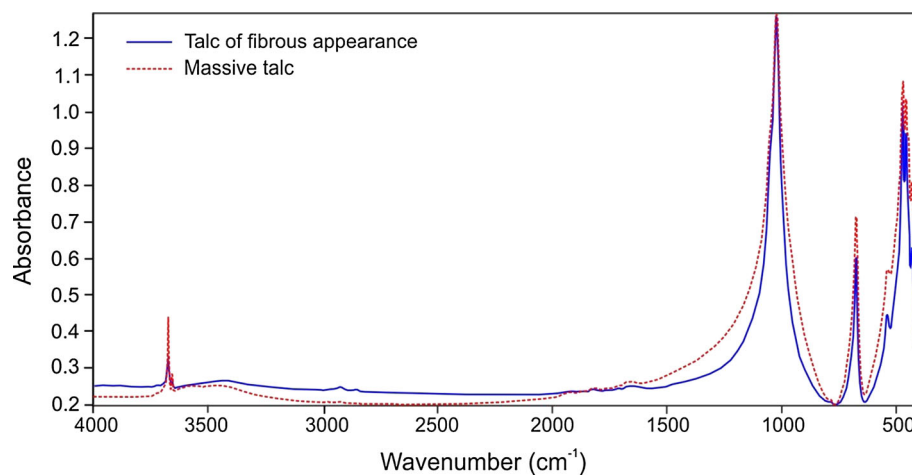
Fig. 7 DSC–TGA diagrams of talc with fibrous appearance (**a**) and massive talc (**b**)

Fig. 8 FTIR diagrams of talc of fibrous appearance and massive talc

Morphological characterization

In order to verify the presence of fibrous morphologies and determine the size of the fibres to evaluate their potential hazardousness, the talc of fibrous appearance in veins and the tremolite (in tremolite and vermiculite zones) were studied. The talc from veins shows a planar and not fibrous habit (Fig. 9a) in secondary electron images (SEM). It

Table 4 Assignment of absorption bands (cm^{-1}) for talc of fibrous appearance and massive talc determined by FTIR

Absorption bands (cm^{-1})		Assignment
Talc of fibrous appearance	Massive talc	
3676.83	3676.75	OH stretching (Mg$_3$–OH)
3660. 48	3660. 38	OH stretching (Mg$_2$Fe–OH)
–	3567.88	Interlayer OH stretching (SiOSi)–OH
3429.19	3453.00	Interlayer OH stretching (SiOAl)–OH
2925.18	–	Probable organic contamination
2855.36	–	Probable organic contamination
1641.91	1645.18	Probable adsorbed water in the sample
1016.82	1016.52	Si–O–Si stretching
669.30	669.44	OH bending
534.40	532.61	Si–O–Mg vibration
464.54	464.45	Mg–O vibration
450.71	450.49	Si–O–Mg vibration
424.90	424.45	Si–O vibration

appears as plates (~ 300–100 μm) stacked and more or less flexed. Some crystals are thinner (~ 20–10 μm) with irregular ends (Fig. 9b). Therefore, the fibrous appearance observed at macroscopic (in the field and with stereomicroscopy) and microscopic level (on thin sections by optical microscopy, SEM and EPMA) actually corresponds to an apparent habit resulting from the orientation of the sample (perpendicular to the talc packets).

Regarding the morphology of tremolite, 50 crystals in the vermiculite and tremolite zones were analysed, complementing the measurements with petrographic observations on thin sections and SEM on natural surfaces.

Finally, the values of both populations were plotted in a width versus aspect ratio diagram (Fig. 10). In the tremolite zone, the elongated prismatic crystals predominate (Fig. 9c, d), their dimensions being in a range of ~ 3.5 mm to 450 μm in length and ~ 500 to 40 μm in diameter. In general, they have irregular ends due to the intense cracking perpendicular to the direction of major elongation of the crystals. Fractures are also observed in the direction of their growth on the planes of cleavage (longitudinal).

In the vermiculite zone, fibrous crystals of smaller diameter and length (~ 250–9 μm long and ~ 9–0.2 μm in diameter) are mainly associated with the vermiculite sheets and the carbonates of this sector (Fig. 9e, f). In general, straight-ended fibres predominate, although flexed crystals are also observed. Approximately, 60% of the fibres measured in this zone are above the maximum diameter of 3 μm stipulated by the WHO (1986) and 40% below that value. About 82% of the latter fibres have diameters ≤ 1.5 μm, i.e. ~ 33% of the fibres in the vermiculite zone have these dimensions.

Discussion

In the Rosarito mine, talc veins of fibrous appearance are observed, with crystals growing towards the interior. However, through SEM on natural surfaces of the samples, it was determined that the habit of the crystals is planar, forming packets of superimposed sheets. Therefore, the fibrous appearance observed at macroscopic (in the field and by stereomicroscopy) and microscopic (optical microscopy, SEM and EPMA on polished surfaces) level is an apparent habit due to the orientation of the sample (perpendicular to the talc packets). On the other hand, the studies by optical microscopy, XRD, SEM, EPMA, DSC-TGA and FTIR confirmed the absence of tremolite associated with talc in this zone. Chlorite is the only phase associated in minor amounts.

Talc in the talc–chlorite zone (mine ore) is mainly associated with chlorite and opaque minerals in variable proportions. Relics of antigorite are in very low proportion, as evidenced by XRD, DSC-TGA and FTIR results. They were only recognized by petrography, SEM and EPMA in very discrete sectors.

Harington and Roe (1965) assumed that asbestos carcinogenic effects may also be due to the presence of trace elements (i.e. Cr and Ni). Later Cralley et al. (1968) reported results showing the possible role of Ni, Cr and Mn in the development of asbestos cancers in textile industry workers and bovines. Gross et al. (1969) showed that asbestos dust with high concentrations of Cr, Co and Ni may induce lung cancer. The concentration of trace elements is highly variable due to the different geochemical processes involved in their formation. Bloise et al. (2016a) reported that the pathogenic effects of asbestos are related
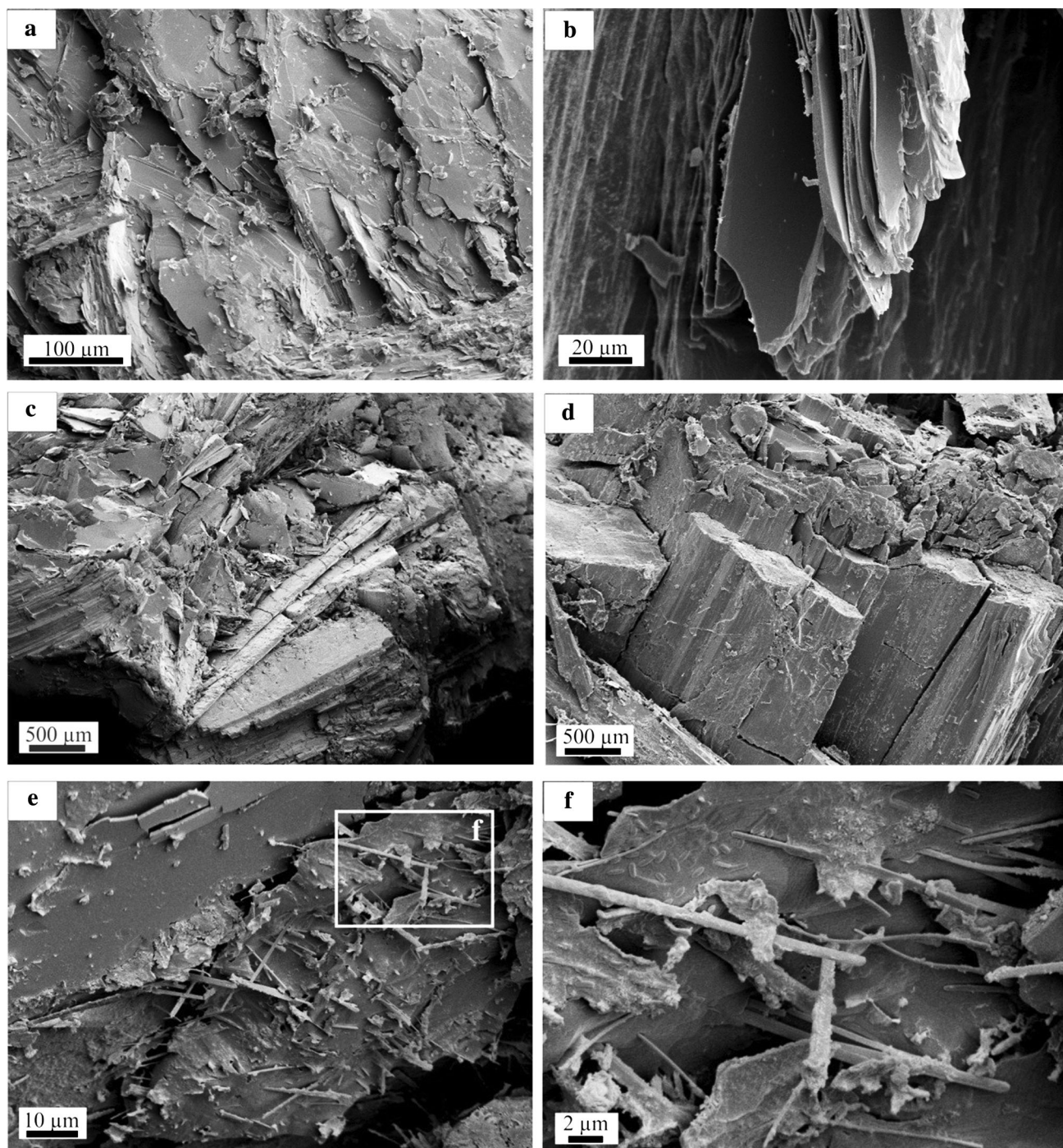
Fig. 9 Secondary electron images (SEM). a Superimposed talc sheets. b Irregular end of fragments of talc sheets. c Elongated tremolite prisms in Tr zone. d Basal sections of tremolite prisms in Tr zone. e Fibrous tremolite in Vrm zone. f Detail of tremolite fibres in the sector "f" of 10e. Straight and finer fibres are observed

to the dimension, biopersistence and chemical composition of the fibres.

The Cr_2O_3 and NiO contents at the centre and edge of prismatic and acicular amphibole crystals in the Tr–Chl–Tlc zone in the Rosarito mine are variable, reaching values of 0.13 and 0.11 wt%, respectively.

Tremolite develops mainly in three sectors of the outcrop, namely in the tremolite–chlorite zone, tremolite–chlorite–talc zone and in contact with the granitic intrusive (tremolite and vermiculite zones). In the first two ones, tremolite appears as euhedral prisms, elongated to acicular, from 250 μm to 1.5 mm in length and 10–250 μm in
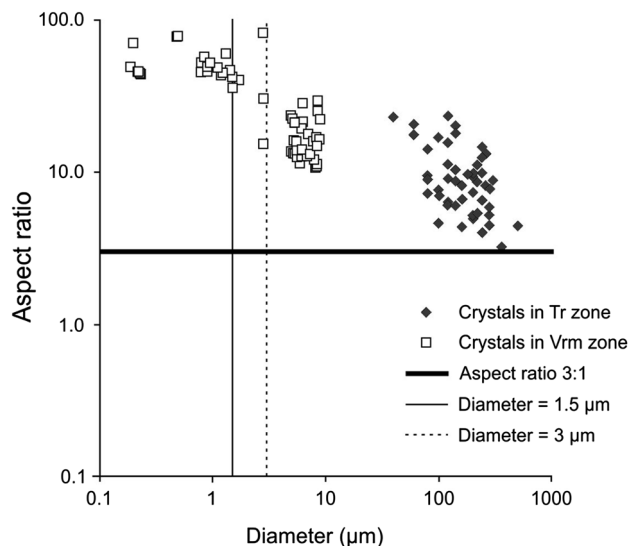
Fig. 10 Comparative graph (diameter vs. aspect ratio) of tremolite crystals in Tr and Vrm zones

diameter. The diameter is well above that corresponding to respirable particles (WHO 1986).

The crystals are generally highly fractured both transversely to the greater elongation of the prisms and longitudinally in the directions of cleavage.

Considering that these sectors are in contact with the talc–chlorite zone, materials rich in prismatic amphiboles could be incorporated during grinding and potentially generate cleavage fragments (non-asbestiform according to Gunter et al. 2007) with dimensions within of the range of respirable particles. Although their hazardousness has been discussed (Mossman 2008; Williams et al. 2013), it is a topic that should be addressed for this type of mine.

In the tremolite zone (close to the vermiculite zone), the crystals have prismatic elongated to acicular habit and reach larger sizes than those observed in tremolite–chlorite and tremolite–chlorite–talc zones (~ 450 μm to 3.5 mm in length and 40–500 μm in diameter), with aspect ratios between 3 and 23. These diameters are also outside the range of respirable particles (Fig. 10).

Finally, in the vermiculite zone, fibrous, straight and flexed tremolite crystals in two groups of contrasted dimensions were observed. The first ones, with diameters >3 μm and therefore outside the range of respirable particles (l: ~ 67–250 μm, d: ~ 5–9 μm, l/d: 11–29), represent $\sim 60\%$ of the fibres in this zone. The second ones, with diameters <3 μm (l: 9.3–227 μm, d: ~ 0.19–2.8 μm, l/d: 15–81), considered as respirable fibrous particles according to the criteria of the WHO (1986), account for $\sim 40\%$ of the fibres in the zone.

In addition, $\sim 33\%$ of the fibres in the vermiculite zone have diameters ≤ 1.5 μm and lengths >9 μm with aspect ratios >20 ($l \sim 9.3$–78 μm, $d \sim 0.19$–1.5 μm, l/d 36–78),

so they can be considered the most dangerous (ERG 2003) or those most prone to cause carcinogenic pathologies (Fig. 10).

Although fibres with smaller diameters (e.g. <0.4 μm, Berman and Crump 2008, <0.25 μm, Stanton et al. 1981) would pose a greater health risk, the definition of a limit close to 1.5 μm allows including in the count fibres that, although they may be less harmful, also have the potential to produce harmful effects. So this criterion has been adopted by several authors not only as a limit for respirable particles, but also to differentiate asbestiform and non-asbestiform particles (e.g. <1 μm, Harper et al. 2008; <1.5 μm, Chatfield 2008; Berman 2010, 2011). It is important to note that these tremolite crystals appear as individual long and thin fibres (straight and flexed) grouped in discrete sectors and not as bundles of fibres that can split lengthwise. Then, although they have dimensions to be considered as asbestiform fibres (according to the WHO criteria), they do not meet the definition of asbestiform morphology, as was already observed by Gunter et al. (2007) in vermiculite ores.

The presence of asbestiform minerals associated with vermiculite is well documented. Perhaps the most well-known case is that of the Libby mine in Montana in the USA (e.g. Sullivan 2007; Gunter et al. 2006, 2008; Antao et al. 2012) where asbestiform tremolite and other fibrous amphiboles were present.

The asbestiform fibres are located between the vermiculite sheets and can be released during mining and grinding, as well as during quick thermal treatments (thermal exfoliation) that can increase more than 20 times the vermiculite volume (Heller-Kallai 2006).

The presence of fibrous amphibole in vermiculite deposits in the province of Córdoba (Lescano et al. 2011, 2013, 2014) has highlighted a problem that has been little discussed in Argentina. So it is necessary to continue the studies on both vermiculite production and potential vermiculite mines. In addition, although no asbestiform minerals associated with talc ore were identified in the Rosarito mine, their presence in talc deposits has been widely documented (Van Gosen et al. 2004). So comprehensive studies aiming to determine the presence of asbestiform minerals in meta-ultramafic rocks of the region must be conducted.

From previous work in the area (Martino et al. 2010; Anzil et al. 2014 and references therein) as well as from field observations and the studies on the collected samples, some inferences can be made. The ultramafic body was serpentinized and affected by medium to high-grade metamorphism resulting in the formation of a tremolite–chlorite schist (clinochlore 1 rich in Fe, Cr and Ni) leaving only antigorite relics. At this stage, the tremolite and biotite zones could have formed by metasomatic processes

(later altered to vermiculite) in contact with the gneiss host ("blackwall") (Barnes et al. 2004). The complex was then affected by high temperature deformation shear zones evidenced mainly in the gneiss, which is milonitized in some sectors.

This event may have been followed by decompression and cooling in amphibolite facies, which could have generated the largest tremolite crystals (tremolite 1–6 rich in Cr and Ni) in the ultramafic body. Subsequently, there may have been a retrograde cooling and hydration event with lower temperature fluids that affected both the ultrabasic body and the host rock, forming discordant talc and calcite veins.

The main body steatization may have occurred at this stage, concentrating in areas of weakness. The fluids could have favoured the replacement of chlorite by talc and probably of tremolite by chlorite both in the ore areas and on both sides of the talc veins. This alteration may have been transitional, from the ore zone to the Tr–Chl–Tlc zone.

The composition of talc (rich in Fe and Ni) is similar to that reported by other authors (e.g. Evans and Trommsdorff 1974; El-Sharkawy 2000; Karlsen et al. 2000) and is consistent with an alteration model of ultramafic rocks.

Finally, there may have been an intrusion of the granite body that could have generated intense hydrothermal activity with fluids rich in Si and K, which could have formed biotite from ultrabasic rock minerals, then altered to vermiculite both in the contact zone and in other planes of weakness of the rock (and additionally quartz veins). This scheme of biotite generation by granitic intrusive bodies and subsequent alteration to vermiculite in ultramafic rocks has been described by other authors (Tsirambides and Michailidis 1999). The presence of vermiculite not only in the contact zone but also in discrete bands that crosscut the serpentinized and steatized body favours the hypothesis of vermiculite formation during this stage.

However, complementary studies (geochemical, isotopic, thermobarometric, etc.) are necessary to gain further knowledge about the processes involved in the mineralization of rocks in the Rosarito mine and to be able to extrapolate the results to other areas with similar characteristics.

Conclusions

From a multimethodological study on the different alteration zones of the rocks in the Rosarito mine (province of Córdoba, Argentina), the following conclusions were reached:

- The talc identified in veins has laminar and non-fibrous habit. The fibrous appearance observed both in the field and by microscopy is an apparent habit due to the orientation of the sample. The study of secondary electron images by SEM is essential to avoid erroneous interpretations.
- Although tremolite was recognized in tremolite–chlorite, tremolite–chlorite–talc zones and in contact with the granitic intrusive (tremolite and vermiculite zone), only $\sim 40\%$ of those located in the vermiculite zone have dimensions to be considered as asbestiform fibres in the range of respirable particles.
- The results show that it is necessary not only to establish concrete definitions for the terminology used, especially in the studies of asbestiform morphology fibres in natural environments, but also for their dimensions and hazardousness. In the bibliography there are different morphometric proposals, so the results can vary depending on the criterion applied.
- Considering that there are records on the presence of asbestiform minerals in other areas of the province of Córdoba (Argentina), multimethodological approaches will be continued in order to develop a model that may be applicable to other ultramafic bodies with similar characteristics.

References

American Council on Science and Health (ACSH) (2007) Asbestos exposure: how risky is it?. American Council on Science and Health Inc, New York, p 33

Antao VC, Larson TC, Horton DK (2012) Libby vermiculite exposure and risk of developing asbestos-related lung and pleural diseases. Curr Opin Pulm Med 18(2):161–167. doi:10.1097/MCP.0b013e32834e897d

Anzil PA, Guereschi AB, Martino RD (2014) Las rocas ultramáficas de las Sierras de Córdoba. In: Martino RD, Guereschi AB (eds) Geología y Recursos Naturales de la Provincia de Córdoba, Relatorio del 19° Congreso Geológico Argentino, 1st edn. Asociación Geológica Argentina, Córdoba, pp 129–150

Barnes JD, Selverstone J, Sharp ZD (2004) Interactions between serpentinite devolatilization, metasomatism and strike-slip strain localization during deep-crustal shearing in the Eastern Alps. J Metamorph Geol 22(4):283–300. doi:10.1111/j.1525-1314.2004.00514.x

Berman DW (2003) Analysis and interpretation of measurements for the determination of asbestos in core samples collected at the Southdown quarry in Sparta, New Jersey. Prepared for the U.S.

Environmental Protection Agency, Region 2 and the New Jersey Department of Environmental Protection. pp 1–53

Berman DW (2010) Comparing milled fiber, Quebec ore, and textile factory dust: has another piece of the asbestos puzzle fallen into place? Crit Rev Toxicol 40(2):151–188. doi:10.3109/10408440903349137

Berman DW (2011) Apples to apples: the origin and magnitude of differences in asbestos cancer risk estimates derived using varying protocols. Risk Anal 31(8):1308–1326. doi:10.1111/j.1539-6924.2010.01581.x

Berman DW, Crump KS (2003) Final draft: technical support document for a protocol to assess asbestos-related risk. Office of Solid Waste and Emergency Response, U.S. Environmental Protection Agency, Washington, DC, EPA #9345.4-06

Berman DW, Crump KS (2008) A meta-analysis of asbestos-related cancer risk that addresses fiber size and mineral type. Crit Rev Toxicol 38(S1):49–73. doi:10.1080/10408440802273156

Bloise A, Critelli T, Catalano M, Apollaro C, Miriello D, Croce A, Barrese E, Liberi F, Piluso E, Rinaudo C, Belluso E (2014) Asbestos and other fibrous minerals contained in the serpentinites of the Gimigliano-Mount Reventino Unit (Calabria, S-Italy). Environ Earth Sci 71(8):3773–3786. doi:10.1007/s12665-013-3035-2

Bloise A, Barca D, Gualtieri A, Pollastri S, Belluso E (2016a) Trace elements in hazardous mineral fibres. Environ Pollut 216:314–323

Bloise A, Punturo R, Catalano M, Miriello D, Cirrincione R (2016b) Naturally occurring asbestos (NOA) in rock and soil and relation with human activities: the monitoring example of selected sites in Calabria (southern Italy). Ital J Geosci 135(2):268–279. doi:10.3301/IJG.2015.24

Bonalumi A, Martino R, Baldo E, Zarco J, Sfragulla JA, Carignano C, Tauber A, Kraemer P, Escayola M, Cabanillas A, Juri E, Torres, B (1999) Hoja Geológica 3166-IV. Villa Dolores. (Memoria y Mapa Geológico). SEGEMAR. Buenos Aires, Boletín 250

Bonalumi A, Sfragulla J, Jerez D, Bertolino S, Sánchez Rial J, Carrizo E (2014) Yacimientos de minerales y rocas industriales. In: Martino RD, Guereschi AB (eds) Geología y Recursos Naturales de la Provincia de Córdoba, Relatorio del 19° Congreso Geológico Argentino, 1st edn. Asociación Geológica Argentina, Córdoba, pp 983–1023

Boulanger G, Andujar P, Pairon J-C, Billon-Galland M-A, Dion C, Dumortier P, Brochard P, Sobaszek A, Bartsch P, Paris C, Jaurand M-C (2014) Quantification of short and long asbestos fibers to assess asbestos exposure: a review of fiber size toxicity. Environ Health 13:59. doi:10.1186/1476-069X-13-59

Brown H, Sigvaldsen J, Singletary H, Lamorte M (1979) Asbestos/rock quarries—mineralogical analysis of crushed stone samples. Office of Air Quality Planning and Standards, U.S. Environmental Protection Agency, Final Report, EPA-450/3-79-031, North Carolina, pp 1–166

Case B, Abraham J, Meeker G, Pooley F, Pinkerton K (2011) Applying definitions of "asbestos" to environmental and "low-dose" exposure levels and health effects, particularly malignant mesothelioma. J Toxicol Environ Health Part B Crit Rev 14(1–4):3–39. doi:10.1080/10937404.2011.556045

Chatfield EJ (2008) A procedure for quantitative description of fibrosity in amphibole minerals. In: Critical issues in monitoring asbestos, 2008 ASTM Johnson conference. ASTM International, Burlington, Vermont, July 14–July 18, 2008. http://www.cdc.gov/niosh/docket/archive/docket099C.html

Cralley LJ, Keenan RG, Kupel RE, Kinser RE, Lynch JR (1968) Characterization and solubility of metals associated with asbestos fibers. Am Ind Hyg Assoc J 29:569–573

Cuervo S (1988) Analisis multivariado de algunas manifestaciones talcosas de la Sierra de Cordoba. Trabajo Final, Universidad Nacional de Córdoba (unpublished), Córdoba, p 143

Dodson RF, Atkinson MA, Levin JL (2003) Asbestos fiber length as related to potential pathogenicity: a critical review. Am J Ind Med 44(3):291–297. doi:10.1002/ajim.10263

Eastern Research Group, Inc. (ERG) (2003) Report on the peer consultation workshop to discuss a proposed protocol to assess asbestos-related risk. Final report. Prepared for the Office of Solid Waste and Emergency Response, U.S. Environmental Protection Agency, Washington, DC, p 279

El-Sharkawy MF (2000) Talc mineralization of ultramafic affinity in the Eastern Desert of Egypt. Miner Deposita 35(4):346–363. doi:10.1007/s001260050246

Evans BW, Trommsdorff V (1974) Stability of enstatite + talc, and CO_2-metasomatism of metaperidotite, Val d'Efra, Lepontine Alps. Am J Sci 274(3):274–296. doi:10.2475/ajs.274.3.274

Földvári M (2011) Handbook of thermogravimetric system of minerals and its use in geological practice. Occasional papers of the Geological Institute of Hungary, vol 213. Geological Institute of Hungary, Budapest, p 180

Giacomini F, Boerio V, Polattini S, Tiepolo M, Tribuzio R, Zanetti A (2010) Evaluating asbestos fibre concentration in metaophiolites: a case study from the Voltri Massif and Sestri-Voltaggio Zone (Liguria, NW Italy). Environ Earth Sci 61:1621–1639. doi:10.1007/s12665-010-0475-9

Gibbons W (1998) The exploitation and environmental legacy of amphibole asbestos: a late 20th century overview. Environ Geochem Health 24(4):213–230. doi:10.1023/A:1006562102206

Gross P, deTreville RT, Tolker EB, Kaschak M, Babyak MA (1969) The pulmonary macrophage response to irritants: an attempt at quantitation. Arch Environ Occup Health 18:174–185

Gunter ME, Williams TJ, Sanchez MS, Harris KE, Bunker KL, Wyss RK, Lee RJ (2006) Amphiboles between the sheets: an interesting occurrence with even more interesting morphologies. Geol Soc Am Abstr Programs 38(7):114

Gunter ME, Belluso E, Mottana A (2007) Amphiboles: environmental and health concerns. In: Hawthorne FC, Oberti R, Ventura GD, Mottana A (eds) Amphiboles: crystal chemistry, occurrence, and health issues. Reviews in mineralogy and geochemistry, vol 67, no 1, pp 453–516. doi:10.2138/rmg.2007.67.12

Gunter ME, Harris KE, Bunker KL, Wyss RK, Lee RJ (2008) Amphiboles between the sheets: observations of interesting morphologies by TEM and FESEM. Eur J Miner 20(6):1035–1041. doi:10.1127/0935-1221/2008/0020-1872

Harington JS, Roe F (1965) Studies of carcinogenesis of asbestos fibers and their natural oils. Ann NY Acad Sci 132:439–450

Harper M (2008) 10th Anniversary critical review: naturally occurring asbestos. J Environ Monit 10(12):1394–1408. doi:10.1039/b810541n

Harper M, Lee EG, Doorn SS, Hammond O (2008) Differentiating non-asbestiform amphibole and amphibole asbestos by size characteristics. J Occup Environ Hyg 5(12):761–770. doi:10.1080/15459620802462290

Heller-Kallai L (2006) Thermally modified clay minerals. In: Bergaya F, Theng BKG, Lagaly G (eds) Handbook of clay science, developments in clay science, vol 1, 1st edn, Chapter 7.2. Elsevier, Amsterdam, pp 289–308. doi:10.1016/S1572-4352(05)01009-3

Karlsen TA, Rian E, Olesen O (2000) Overview of talc resources in the Altermark talc province, northern Norway, and possible uses of the talc ore. NGU Bull 436:93–102

Lee RJ, Strohmeier BR, Bunker KL, Van Orden DR (2008) Naturally occurring asbestos: a recurring public policy challenge. J Hazard Mater 153(1–2):1–21. doi:10.1016/j.jhazmat.2007.11.079

Lescano L, Marfil S, Maiza P, Sfragulla J, Bonalumi A (2011) Presence of asbestiform minerals in vermiculite. Province of Córdoba, Argentina. In: Environmental geosciences and engineering survey for territory protection and population safety, international conference (EngeoPro 2011), Moscú, Russia, pp 770–774

Lescano L, Marfil S, Maiza P, Sfragulla J, Bonalumi A (2013) Amphibole in vermiculite mined in Argentina. Morphology, quantitative and chemical studies on the different phases of production and their environmental impact. Environ Earth Sci 70(4):1809–1821. doi:10.1007/s12665-013-2268-4

Lescano L, Bonalumi A, Maiza P, Sfragulla A, Marfil S (2014) Asbestiform amphiboles in a serpentinite quarry in operation, province of Córdoba, Argentina. In: Lollino G, Manconi A, Guzzetti F, Culshaw M, Bobrowsky P, Luino F (eds) Engineering geology for society and territory—volume 5: urban geology, sustainable planning and landscape exploitation. Springer Int Pub, Torino, Italy, pp 615–618. doi:10.1007/978-3-319-09048-1_119

Lippmann M (1988) Asbestos exposure indices. Environ Res 46(1):86–106. doi:10.1016/S0013-9351(88)80061-6

Lippmann M (1994) Deposition and retention of inhaled fibres: effects on incidence of lung cancer and mesothelioma. Occup Environ Med 51(12):793–798

Lippmann M (2009) Asbestos and other mineral and vitreous fibers. In: Lippmann M (ed) Environmental toxicants: human exposures and their health effects, 3rd edn. Wiley, New Jersey, pp 395–458

Locock AJ (2014) An excel spreadsheet to classify chemical analyses of amphiboles following the IMA 2012 recommendations. Comput Geosci 62:1–11. doi:10.1016/j.cageo.2013.09.011

Loomis D, Dement J, Richardson D, Wolf S (2010) Asbestos fibre dimensions and lung cancer mortality among workers exposed to chrysotile. Occup Environ Med 67(9):580–584. doi:10.1136/oem.2009.050120

Marescotti P, Crispini L, Poggi E, Capponi G, Solimano M (2014) The asbestos risk in meta-ophiolitic rocks: a protocol for preliminary field and laboratory investigations during geological mapping. In: Lollino G, Manconi A, Guzzetti F, Culshaw M, Bobrowsky P, Luino F (eds) Engineering geology for society and territory—volume 5: urban geology, sustainable planning and landscape exploitation, Springer Int Pub, Torino, Italy, pp 623–626. doi:10.1007/978-3-319-09048-1_121

Markowitz S (2015) Asbestos-related lung cancer and malignant mesothelioma of the pleura: selected current issues. Semin Respir Crit Care Med 36(3):334–346. doi:10.1055/s-0035-1549449

Martino RD, Guereschi AB, Anzil PA (2010) Metamorphic and tectonic evolution at 31°36′S across a deep crustal zone from the Sierra Chica of Córdoba, Sierras Pampeanas, Argentina. J S Am Earth Sci 30(1):12–28. doi:10.1016/j.jsames.2010.07.008

Mossman BT (2008) Assessment of the pathogenic potential of asbestiform vs. nonasbestiform particulates (cleavage fragments) in in vitro (cell or organ culture) models and bioassays. Regul Toxicol Pharmacol 52(1):S200–S203. doi:10.1016/j.yrtph.2007.10.004

Mossman BT, Lippmann M, Hesterberg TW, Kelsey KT, Barchowsky A, Bonner JC (2011) Pulmonary endpoints (lung carcinomas and asbestosis) following inhalation exposure to asbestos. J Toxicol Environ Health B Crit Rev 14(1–4):76–121. doi:10.1080/10937404.2011.556047

Occupational Safety and Health Administration (OSHA) (1992) Occupational exposure to asbestos, tremolite, anthophyllite and actinolite (29 CFR Parts 1910 and 1926—final rules). US Department of Labor Federal Register 57(110):24310–24331

Parry SA, Pawley AR, Jones RL, Clark SM (2007) An infrared spectroscopic study of the OH stretching frequencies of talc and

10-Å phase to 10 GPa. Am Miner 92(4):525–531. doi:10.2138/am.2007.2211

Petit S, Martin F, Wiewiora A, De Parseval P, Decarreau A (2004) Crystal-chemistry of talc: a near infrared (NIR) spectroscopy study. Am Miner 89(2–3):319–326

Resolution N°577/1991 (1991) Ministerio de Trabajo y Seguridad Social, Argentina, Boletín oficial No 27.176 1ra Sección, pp 5–11

Resolution N°823/2001 (2001) Ministerio de Salud de la Nación, Argentina, Boletín oficial No 29.700 1ra Sección, pp 10–11

Resolution N°845/2000 (2000) Ministerio de Salud de la Nación, Argentina, Boletín oficial No 29.505 1ra Sección, pp 6–7

Rigopoulos I, Tsikouras B, Pomonis P, Karipi S, Hatzipanagiotou K (2010) Quantitative analysis of asbestos fibres in ophiolitic rocks used as aggregates and hazard risk assessment for human health. Bull Geol Soc Greece 43(5):2712–2725

Rodriguez EJ (2004) Asbestos banned in Argentina. Int J Occup Environ Health 10(2):202–208. doi:10.1179/oeh.2004.10.2.202

Ross M, Nolan RP (2003) History of asbestos discovery and use and asbestos-related disease in context with the occurrence of asbestos within ophiolite complexes. In: Dilek Y, Newcomb S (eds) Ophiolite concept and the evolution of geological thought. The Geological Society of America, Boulder, Colorado, Special paper 373, pp 447–470. doi:10.1130/0-8137-2373-6.447

Ross M, Nolan RP, Langer AM, Cooper WC (1993) Health effects of mineral dusts other than asbestos. In: Guthrie GD, Mossman BT (eds) Health effects of mineral dusts, reviews in mineralogy, chapter 12. Mineralogical Society of America, Washington, DC 28: 361–408

Sanchez VC, Pietruska JR, Miselis NR, Hurt RH, Kane AB (2009) Biopersistence and potential adverse health impacts of fibrous nanomaterials: what have we learned from asbestos? WIREs Nanomed Nanobiotechnol 1(5):511–529. doi:10.1002/wnan.41

Sfragulla JA, Moreno RS (1985) Mapa geológico minero de la mina Rosarito, Departamento Punilla. Secretaría de Minería Córdoba (unpublished)

Stanton MF, Layard M, Tegeris A, Miller E, May M, Morgan E, Smith A (1981) Relation of particle dimension to carcinogenicity in amphibole asbestoses and other fibrous minerals. J Natl Cancer Inst 67(5):965–975. doi:10.1093/jnci/67.5.965

Sullivan PA (2007) Vermiculite, respiratory disease, and asbestos exposure in Libby, Montana: update of a cohort mortality study. Environ Health Perspect 115(4):579–585. doi:10.1289/ehp.9481

Tan H, Skinner W, Addai-Mensah J (2012) Leaching behaviour of low and high fe-substituted chlorite clay minerals at low pH. Hydrometallurgy 125–126:100–108. doi:10.1016/j.hydromet.2012.05.015

Tsirambides A, Michailidis K (1999) An X-ray, EPMA, and oxygen isotope study of vermiculitized micas in the ultramafic rocks at Askos, Macedonia, Greece. Appl Clay Sci 14(1–3):121–140. doi:10.1016/S0169-1317(98)00054-4

Van Gosen BS, Lowers HA, Sutley SJ, Gent CA (2004) Using the geologic setting of talc deposits as an indicator of amphibole asbestos content. Environ Geol 45(7):920–939. doi:10.1007/s00254-003-0955-2

Vignaroli G, Rossetti F, Belardi G, Billi A (2011) Linking rock fabric to fibrous mineralisation: a basic tool for the asbestos hazard. Nat Hazards Earth Syst Sci 11:1267–1280. doi:10.5194/nhess-11-1267-2011

Vignaroli G, Ballirano P, Belardi G, Rossetti F (2014) Asbestos fibre identification vs. evaluation of asbestos hazard in ophiolitic rock mélanges, a case study from the Ligurian Alps (Italy). Environ Earth Sci 72(9):3679–3698. doi:10.1007/s12665-014-3303-9

Villieras F, Yvon J, Cases JM, De Donato P, Lhote F, Baeza R (1994) Development of microporosity in clinochlore upon heating.

Clays Clay Miner 42(6):679–688. doi:10.1346/CCMN.1994.0420604

Wesolowski M (1984) Thermal decomposition of talc: a review. Thermochim Acta 78(1–3):395–421. doi:10.1016/0040-6031(84)87165-8

Whitney DL, Evans BW (2010) Abbreviations for names of rock-forming minerals. Am Miner 95(1):185–187. doi:10.2138/am.2010.3371

Williams C, Dell L, Adams R, Rose T, Van Orden D (2013) State-of-the-science assessment of non-asbestos amphibole exposure: is there a cancer risk? Environ Geochem Health 35(3):357–377. doi:10.1007/s10653-012-9500-0

World Health Organization (WHO) (1986) Asbestos and other natural mineral fibres. International programme on chemical safety. World Health Organization, Geneva. Environmental Health Criteria, 53

Wylie AG, Candela PA (2015) Methodologies for determining the sources, characteristics, distribution, and abundance of asbestiform and nonasbestiform amphibole and serpentine in ambient air and water. J Toxicol Environ Health Part B 18(1):1–42. doi:10.1080/10937404.2014.997945

Yavuz F, Kumral M, Karakaya N, Karakaya MÇ, Yıldırım DK (2015) A Windows program for chlorite calculation and classification. Comput Geosci 81:101–113. doi:10.1016/j.cageo.2015.04.011